

Dynamics of the excitations of a quantum dot in a microcavity

J.I. Perea, D. Porras, and C. Tejedor

Departamento de Física Teórica de la Materia Condensada,
Universidad Autónoma de Madrid, 28049 Madrid, Spain.

We study the dynamics of a quantum dot embedded in a three-dimensional microcavity in the strong coupling regime in which the quantum dot exciton has an energy close to the frequency of a confined cavity mode. Under the continuous pumping of the system, confined electron and hole can recombine either by spontaneous emission through a leaky mode or by stimulated emission of a cavity mode that can escape from the cavity. The numerical integration of a master equation including all these effects gives the dynamics of the density matrix. By using the quantum regression theorem, we compute the first and second order coherence functions required to calculate the photon statistics and the spectrum of the emitted light. Our main result is the determination of a range of parameters in which a state of cavity modes with poissonian or sub-poissonian (non-classical) statistics can be built up within the microcavity. Depending on the relative values of pumping and rate of stimulated emission, either one or two peaks close to the excitation energy of the dot and/or to the natural frequency of the cavity are observed in the emission spectrum. The physics behind these results is discussed.

PACS numbers: 78.67.Hc, 42.50.Ct

I. INTRODUCTION

Quantum electrodynamics of atoms within optical cavities is a well understood problem which has produced many results of both fundamental and practical interest [1, 2, 3, 4]. The current capability of using semiconductor technology to grow quantum dots (QD) embedded in microcavities seems very promising to reproduce and control that properties in a solid-state system that could be integrated in electronic or optical devices. The essential physics of such system is a strong coupling between the QD excitations and the photonic cavity modes as well as the possibility of interaction with the external world through the pumping of the system and the subsequent emission of light. The main goal is the control of the emitted light and its quantum properties being possible to build up high efficiency light emitting diodes, low threshold lasers and single photon sources.

We concentrate here in a problem, no far from the actual situation in several experiments [5, 6, 7, 8, 9, 10, 11], in which a single QD is embedded in a pillar or disk microcavity confining photons in the three spatial directions. The system is pumped either by electrically injecting electrons and holes which tunnel into the QD [6], or by pumping excitons in the QD [5, 7, 9, 10, 11]. Light emission from the system takes place both by cavity mode decay or by spontaneous emission of leaky modes. All these pumping and emission mechanisms introduce decoherence affecting the quantum properties of the system.

The lowest energy excitation of a neutral QD is an electron-hole pair, usually labelled as exciton. Due to the fermionic character of its components, this exciton

state can only be singly occupied having a degeneracy related to the possible values of the third component of the total angular momentum. This quantum number is usually referred to as the spin of the exciton. Among all these states, only two cases, those corresponding to

1, are of interest in our problem due to their possible coupling with photons. The next excitation corresponds to the case in which both +1 and -1 excitons are occupied. This biexciton state has an energy different to twice that of a single exciton due to the Coulomb interaction of their components. This spectrum presents interesting alternatives [12] that we intend to study in future work while here we restrict to simplest case, in which we consider only excitons with a given spin. This assumption is well justified in the case of experiments in which the system is pumped with polarized light, so that excitons with a given angular momentum are created in the system. We also assume that spin flip mechanisms are slow as compared with typical time scales in our system. Other single-particle states of the QD, above the exciton energy, can be neglected because they are not strongly coupled to the cavity mode in the case of resonance or quasi-resonance between the exciton and the confined photon. Under these conditions, the problem reduces to that of a two-level artificial atom embedded in the optical cavity. We are going to show that, in spite of this simplification, the system presents a very rich variety of physical situations.

The problem of a two-level system coupled to a single cavity mode, under different conditions and approximations, has received a lot of attention, mainly in the field of quantum optics [1, 2, 3, 4, 13, 14]. Of particular interest is the study of the possible sub-poissonian radiation when cavity losses and pumping dominate onto the spontaneous emission of leaky modes. The aim of our work is an exhaustive analysis of the different regimes of parameters to determine the role played by the different

Present address: Max-Planck Institute for Quantum Optics, D-85748, Garching, Germany.

physical mechanisms in the quantum properties of both the internal state of the system and the light emitted in the steady regime under continuous incoherent pumping.

The paper is organized as follows: In section II we describe the model Hamiltonian and master equation that allows to calculate the evolution of the populations and coherences of the energy levels. By means of the quantum regression theorem, we can use our master equation to calculate cavity photon statistics and the spectrum of the emitted light. In section III we present the results for the time evolution of the magnitudes of interest, in different ranges of parameters characterizing different physical situations. The spectrum of the light emitted by the system is presented and discussed in section IV. Section V is devoted to a summary of the work.

II. THEORETICAL FRAMEWORK

We consider a single QD inside a semiconductor microcavity that is continuously and incoherently pumped. Our system is initially in its ground state and evolves until it reaches the steady-state. In order to describe the time evolution of the QD-cavity system we use a master equation that includes the strong exciton-photon coupling, the non-resonant pump, and the interaction with the environment that is responsible for dissipation.

A. The Hamiltonian

The physics of a QD strongly coupled with a single cavity mode is described by the following Hamiltonian:

$$H = H_S + H_{RS} + H_R \quad (1)$$

H_S , H_R are the Hamiltonian for the QD-cavity system, and the environment (reservoirs), respectively. The term H_{RS} describes the interaction between the QD-cavity system and the reservoirs. H_S is given by the usual Jaynes-Cummings Hamiltonian [2, 4] that describes the interaction of a two-level system with a single mode of the electromagnetic field:

$$\begin{aligned} H_S &= H_0 + H_{XC} \\ H_0 &= \sum_x \hbar \omega_x |x\rangle\langle x| + \sum_x \hbar \omega_x |x\rangle\langle x| a^\dagger a \\ H_{XC} &= g (a^\dagger + a) \end{aligned} \quad (2)$$

We have introduced ladder operators $a^\dagger = \sum_j |j+1\rangle\langle j|$, $a = \sum_j |j\rangle\langle j+1|$ connecting the ground $|0\rangle$ and excited (exciton) $|x\rangle$ states of the QD with energies zero and $\hbar\omega_x$ respectively (we take $\hbar = 1$). a^\dagger creates a cavity photon with energy $\hbar\omega_x$. The coupling term H_{XC} in Eq. (2) describes the exciton-photon coupling in the Rotating Wave Approximation [1, 2, 3].

H_{RS} contains the coupling to external reservoirs including the following three process:

- (i) The continuous and incoherent pumping of the QD by annihilating (c_{R^0}) an electron-hole pair from an external reservoir R^0 (representing either electrical injection or the capture of excitons optically created at frequencies larger than the typical ones of our system) and creation ($d_{R^0}^\dagger$) a phonon emitted to a reservoir R^0 in order to take care of energy conservation

$$\sum_{R^0, R^0} X_{R^0, R^0} [d_{R^0}^\dagger c_{R^0} + c_{R^0}^\dagger d_{R^0}]; \quad (3)$$

- (ii) The direct coupling of the QD exciton to the leaky modes, that is, to the photonic modes, with energy different than the cavity mode, that have a residual density of states inside the microcavity. This process is responsible for the dissipation of the excitonic degrees of freedom by the spontaneous emission to an external reservoir R of photons created by b_R^\dagger

$$\sum_R X_{R, R} [b_R^\dagger + b_R]; \quad (4)$$

- (iii) The escape of the cavity mode out of the microcavity due to the incomplete reflectance of the mirrors. The cavity mode is thus coupled to the continuum of photonic modes out of the microcavity. This process produces the direct dissipation of the cavity mode

$$H_{CE} = \sum_R X_{R, R} (a b_R^\dagger + b_R a^\dagger); \quad (5)$$

The last term in Eq. (1), H_R , describes the external reservoirs of harmonic oscillators (photons, phonons, electron-hole pairs,...) not being necessary to detail them explicitly. The three terms H_{RS} have coupling constants \sum_{R^0, R^0} , \sum_R and \sum_R which depend on the particular mode (R , R^0 or R^0) of each external reservoir. The operators a , b_R , c_{R^0} and d_{R^0} have bosonic commutation rules as it corresponds to harmonic oscillators. Since we are interested in the strong coupling regime, the first three terms, H_0 and H_{XC} are treated exactly. That means that one could work in the framework usually known as the "dressed atom picture". However, in order to clarify the different pumping and losses mechanisms, it is preferable to work in basis $|j\rangle$ in terms of the number of cavity photons n and bare ground G and exciton X states of the QD.

B. Master equation

We have made the whole algebra for a general case in which reservoirs are at finite temperature. However, the main physics already occurs for zero temperature, which is the case we present hereafter in this paper.

We define the reduced density matrix, ρ , for the exciton-photon system by tracing out the reservoir degrees of freedom in the total density matrix ρ_T :

$$\rho = \text{Tr}_R(\rho_T): \quad (6)$$

In the interaction picture with respect to $H_{XC} + H_{RS}$ in Eqs. (1) and (2), ρ satisfies the master equation [2, 3]:

$$\begin{aligned} \frac{d}{dt} \rho = & \frac{i}{\hbar} [\rho; H_S] + \\ & - \frac{\gamma}{2} (2a^\dagger a \rho + \rho a^\dagger a - a^\dagger a \rho - \rho a^\dagger a) + \\ & - \frac{\gamma}{2} (2a a^\dagger \rho + \rho a a^\dagger - a a^\dagger \rho - \rho a a^\dagger) + \\ & \frac{P}{2} (2\rho + \rho a^\dagger a + \rho a a^\dagger): \end{aligned} \quad (7)$$

The master equation is obtained under the usual Born-Markov approximation for the interaction H_{RS} between the QD-cavity system and the reservoirs, but the strong exciton-cavity photon coupling, H_{XC} , is described exactly. γ is the decay of the cavity photon by escaping through the microcavity mirrors, γ is the decay of the QD exciton by the spontaneous emission into leaky modes, and P is the rate of continuous incoherent pumping of the QD exciton. By means of Eq. (7) one can get a set of differential equations that describe the evolution of the populations and coherences of the cavity-QD system. In the basis $\{|G_n\rangle, |X_n\rangle\}$ of product states between QD states and Fock states of the cavity mode, the matrix elements of the reduced density matrix are:

$$\dot{\rho}_{ij;mn} = \rho_{ij;jm} - \rho_{in;jjm} \quad (8)$$

with i, j being either G or X . The diagonal matrix elements $\rho_{Gn;Gn}$, $\rho_{Xn;Xn}$ are the populations of the QD-photon levels, while the non-diagonal terms $\rho_{Gn;Xn-1}$,

$\rho_{Xn-1;Gn}$, describe the coherences between these levels. By taking the matrix elements in Eq. (7) we get, for $T = 0$, the following set of linear differential equations:

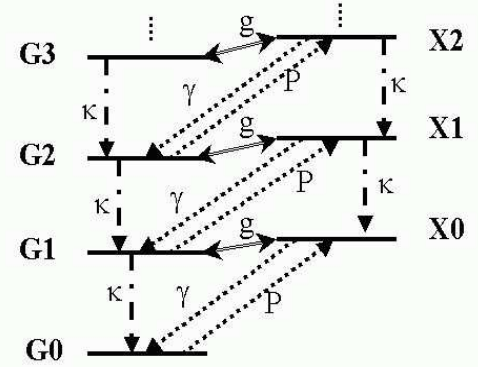


FIG. 1: Ladder of levels (continuous lines) for a two-state QD coupled to a single optical mode of a microcavity. States labeled as G_n with $n = 0, 1, 2, \dots$ correspond to having the QD in its GS coexisting with n cavity photons. The same for states X_n with the QD in its excited state X . The double, dashed and dash-dotted lines depict the coupling, pumping and emission processes with rates g , P , and γ explained in the text.

$$\begin{aligned} \dot{\rho}_{Gn;Gn} = & ig \frac{P}{n} (\rho_{Gn;Xn-1} - \rho_{Xn-1;Gn}) \\ & + \rho_{Xn;Xn} [n \rho_{Gn;Gn} - (n+1) \rho_{Gn+1;Gn+1}] + P \rho_{Gn;Gn} \end{aligned} \quad (9)$$

$$\begin{aligned} \dot{\rho}_{Xn;Xn} = & ig \frac{P}{n+1} (\rho_{Xn;Gn+1} - \rho_{Gn+1;Xn}) \\ & + \rho_{Xn;Xn} [n \rho_{Xn;Xn} - (n+1) \rho_{Xn+1;Xn+1}] + P \rho_{Gn;Gn} \end{aligned} \quad (10)$$

$$\begin{aligned} \dot{\rho}_{Gn;Xn-1} = & ig \frac{P}{n} (\rho_{Gn;Gn} - \rho_{Xn-1;Xn-1}) + \frac{\rho_{Gn;Xn-1}}{n(n+1)} \\ & [(n+1)(2n-1) + P] \rho_{Gn;Xn-1} + \rho_{Gn+1;Xn}; \end{aligned} \quad (11)$$

plus the equation hermitian conjugate of (11). In the absence of dissipation, the matrix elements $\rho_{Gn;Gn}$, $\rho_{Xn-1;Xn-1}$, $\rho_{Gn;Xn-1}$, and $\rho_{Xn-1;Gn}$, for a given photon number n , satisfy a closed set of four differential equations. However, the pumping and emission with rates P , γ , and γ , couple the terms with different photon occupation number n , so that an infinite set of equations has to be solved, as depicted schematically in Fig. 1. For the numerical integration, the set of equations can be truncated at a given value that, in all the cases considered below, it is enough to take equal to 100.

As initial conditions we take $G_{00} = 1$ and all the other elements of the density matrix equal to zero. In other words, we start with the system in its ground state and the pumping, and subsequently the losses, produces the dynamical evolution of the whole system. The steady-state of the system can be studied by integrating the set of equations (9), (10) and (11) for long times.

C. First and second order coherence functions

From the master equation, one can compute the dynamics of the expectation values of any operator. Moreover, two-time correlation functions are also of physical interest. In particular we want to compute the first and second order coherence functions [3, 4]

$$g^{(1)}(\mathbf{r}; t; \tau) = \frac{\langle E^{(+)}(\mathbf{r}; t) E^{(+)}(\mathbf{r}; t + \tau) \rangle}{\langle E^{(+)}(\mathbf{r}; t) E^{(+)}(\mathbf{r}; t) \rangle \langle E^{(+)}(\mathbf{r}; t + \tau) E^{(+)}(\mathbf{r}; t + \tau) \rangle} \quad (12)$$

$$g^{(2)}(\mathbf{r}; t; \tau) = \frac{\langle E^{(+)}(\mathbf{r}; t) E^{(+)}(\mathbf{r}; t + \tau) E^{(+)}(\mathbf{r}; t + \tau) E^{(+)}(\mathbf{r}; t) \rangle}{\langle E^{(+)}(\mathbf{r}; t) E^{(+)}(\mathbf{r}; t) \rangle \langle E^{(+)}(\mathbf{r}; t + \tau) E^{(+)}(\mathbf{r}; t + \tau) \rangle} \quad (13)$$

where $E^{(+)}$ and $E^{(-)}$ are the positive and negative frequency parts of the amplitude of the electromagnetic field. In the steady-state limit we are interested in, both $g^{(1)}$ and $g^{(2)}$ do not depend on the absolute time t .

The experimental situation is such that photonic modes escaping from the cavity are emitted in well defined direction, for instance along the axis of the micropillars in the direction in which the mirrors defining the cavity have some transparency [5, 6, 8, 9, 10, 11]. On the contrary, emission of leaky modes takes place in any direction, particularly through lateral surfaces of the micropillar. This means that simply by changing the spatial distribution of detectors, one can measure the emission from cavity modes or the leaky modes.

By Fourier transforming the first order correlation function

$$G^{(1)}(\mathbf{r}; \omega) = \langle E^{(+)}(\mathbf{r}; \omega) E^{(+)}(\mathbf{r}; \omega) \rangle; \quad (14)$$

one can obtain the power spectrum of the emitted light.

$$S(\mathbf{r}; \omega) = \frac{1}{2\pi} \int_{-\infty}^{\infty} d\tau e^{i\omega\tau} G^{(1)}(\mathbf{r}; \tau); \quad (15)$$

The first order correlation function of the external field can be obtained from the time dependence of the operators describing intrinsic properties of the system:

$$\begin{aligned} G_c^{(1)}(\mathbf{r}; \omega) &= \langle a^\dagger(\omega) a(\omega) \rangle \\ G_x^{(1)}(\mathbf{r}; \omega) &= \langle h^\dagger(\omega) h(\omega) \rangle; \end{aligned} \quad (16)$$

$G_c^{(1)}(\mathbf{r}; \omega)$ is the correlation function for the cavity mode, responsible for the stimulated emission part of the spectrum (i.e. the light coming from the confined photon) by means of $G^{(1)}(\mathbf{r}; \omega) / G_c^{(1)}(\mathbf{r}; \omega)$. In the case of pillar microcavities, it would correspond to the light

emitted in the vertical direction. On the other hand $G_x^{(1)}(\mathbf{r}; \omega)$ describes the spontaneous part of the spectrum (i.e. light directly coupled to the QD exciton) by means of $G^{(1)}(\mathbf{r}; \omega) / G_x^{(1)}(\mathbf{r}; \omega)$. This gives the light emitted through the leaky modes that can be measured in the lateral direction of a micropillar.

In order to calculate these two-time correlation functions, we make use of the quantum regression theorem [2, 3, 4]. First of all, we define the following operators:

$$\begin{aligned} a_{G_n}^\dagger(\omega) &= jG_n + i h G_n j e^{i(\omega - \omega_n)\tau} \\ a_{X_n}^\dagger(\omega) &= jX_n + i h X_n j e^{i(\omega - \omega_n)\tau} \\ h_n^\dagger(\omega) &= jX_n i h G_n j e^{i\omega\tau} \\ h_n(\omega) &= jG_n + i h X_n j e^{i(\omega - \omega_n)\tau}; \end{aligned} \quad (17)$$

In the interaction picture, time evolution with respect to $H_{XC} + H_{RS}$ appears explicitly. The two-time correlation function of the cavity mode can be expressed in terms of these operators:

$$G_c^{(1)}(\mathbf{r}; \omega) = \sum_n \frac{P_n}{\omega - \omega_n + i\gamma} \langle a_{G_n}^\dagger(\omega) a(\omega) + h a_{X_n}^\dagger(\omega) a(\omega) \rangle; \quad (18)$$

The exciton correlation function can be written as:

$$G_x^{(1)}(\mathbf{r}; \omega) = \sum_n \langle h_n^\dagger(\omega) h(\omega) \rangle; \quad (19)$$

For the calculation of the spectrum of the emitted light it is, thus, necessary to evaluate the functions $\langle a_{G_n}^\dagger(\omega) a(\omega) \rangle$, $\langle h a_{X_n}^\dagger(\omega) a(\omega) \rangle$, and $\langle h_n^\dagger(\omega) h(\omega) \rangle$. The quantum regression theorem states that given a set of operators O_j , whose averages satisfy a closed set of linear differential equations:

$$\frac{d}{dt} \langle O_j(t) \rangle = \sum_k L_{jk} \langle O_k(t) \rangle; \quad (20)$$

then the two-time averages of O_j with any other operator O , also satisfy the same differential equation:

$$\frac{d}{dt} \langle O_j(t) O(t) \rangle = \sum_k L_{jk} \langle O_k(t) O(t) \rangle \quad (21)$$

In order to get the time evolution of two-time averages, we start with the dynamics of the operators (17). Their averages satisfy the set of linear differential equations that allows us to find the evolution of the corresponding two-time averages in (19, 19):

$$\begin{aligned} \langle \dot{h}_{G_n}^y \rangle &= \langle \dot{h}_{G_n, G_{n+1}} \rangle e^{i(\dots)} + i(\dots) \langle h_{G_n}^y \rangle \\ \langle \dot{h}_n^y \rangle &= \langle \dot{h}_{G_n, X_n} \rangle e^{i(\dots)} + i(\dots) \langle h_n^y \rangle \\ \langle \dot{h}_{X_{n-1}}^y \rangle &= \langle \dot{h}_{X_{n-1}, X_n} \rangle e^{i(\dots)} + i(\dots) \langle h_{X_{n-1}}^y \rangle \\ \langle \dot{h}_{\kappa_n} \rangle &= \langle \dot{h}_{X_{n-1}, G_{n+1}} \rangle e^{i(\dots)} + i(\dots) \langle h_{\kappa_n} \rangle \end{aligned} \quad (22)$$

Although the operator κ_n is not needed in the evaluation of the required two-time averages (19) and (19), we have to add the correlation functions that include such operator κ_n in order to get a closed set of equations. Using the master equation and eliminating the elements of the density matrix, we arrive at the desired time-evolution for the averages (17):

$$\begin{aligned} \langle \dot{h}_{G_n}^y \rangle &= \langle h_{G_n}^y \rangle i(\dots) - \frac{1}{2} (2n+1) P \\ &+ \langle h_{G_{n+1}}^y \rangle i P \frac{1}{(n+1)(n+2)} + \langle h_n^y \rangle i P \frac{1}{n+1} \\ &+ \langle h_{X_{n-1}}^y \rangle i \langle h_{\kappa_n} \rangle i P \frac{1}{n} \\ \langle \dot{h}_n^y \rangle &= \langle h_{G_n}^y \rangle i P \frac{1}{n+1} + \langle h_n^y \rangle i(\dots) - \frac{1}{2} (P) n \\ &+ \langle h_{n+1}^y \rangle i (n+1) - \langle h_{X_{n-1}}^y \rangle i P \frac{1}{n} \\ \langle \dot{h}_{X_{n-1}}^y \rangle &= \langle h_{G_n}^y \rangle i P \frac{1}{n} \langle h_n^y \rangle i P \frac{1}{n} \\ &+ \langle h_{X_{n-1}}^y \rangle i(\dots) - \frac{1}{2} (2n-1) \\ &+ \langle h_{X_n}^y \rangle i P \frac{1}{n(n+1)} + \langle h_{\kappa_n} \rangle i P \frac{1}{n+1} \\ \langle \dot{h}_{\kappa_n} \rangle &= \langle h_{G_n}^y \rangle i P \frac{1}{n} + \langle h_{X_{n-1}}^y \rangle i P \frac{1}{n+1} \\ &+ \langle h_{\kappa_n} \rangle i(\dots) - \frac{1}{2} (P) n \\ &+ \langle h_{n+1}^y \rangle i P \frac{1}{n(n+2)} \end{aligned} \quad (23)$$

From Eq. (23), and the quantum regression theorem, it is straightforward to obtain two separate closed sets of differential equations for two-time functions: one for the set of functions

$$\langle h_{G_n}^y(t) a(t) \rangle; \langle h_{X_{n-1}}^y(t) a(t) \rangle; \langle h_n^y(t) a(t) \rangle; \langle h_{\kappa_n}(t) a(t) \rangle; \quad (24)$$

needed for the calculation of $G_C^{(1)}(t; \dots)$, and other for the set of functions

$$\langle h_{G_n}^y(t) \rangle; \langle h_{X_{n-1}}^y(t) \rangle; \langle h_n^y(t) \rangle; \langle h_{\kappa_n}(t) \rangle; \quad (25)$$

needed for the calculation of $G_X^{(1)}(t; \dots)$.

An important point is the initial conditions to solve these systems of equations. Such conditions are obtained by

solving, up to the stationary limit, the master equations (9), (10) and (11) for the density matrix. From this infor-

mation, one knows the initial conditions. For the functions in (24):

$$\begin{aligned} h_{Gn}^y(t)a(t)i &= \frac{p}{n+1} G_{n+1;G_{n+1}} \\ h_{X_{n-1}}^y(t)a(t)i &= \frac{p}{n} X_{n;X_n} \\ h_{X_n}^y(t)a(t)i &= \frac{p}{n+1} G_{n+1;X_n} e^{i t} \\ h_{X_n}^y(t)a(t)i &= \frac{p}{n} X_{n;G_{n+1}} e^{i t}; \end{aligned} \quad (26)$$

For the functions in (25):

$$\begin{aligned} h_{Gn}^y(t)a(t)i &= X_{n;G_{n+1}} e^{i t} \\ h_{X_{n-1}}^y(t)a(t)i &= 0 \\ h_{X_n}^y(t)a(t)i &= X_{n;X_n} \\ h_{X_n}^y(t)a(t)i &= 0 \end{aligned} \quad (27)$$

The second order coherence function is, a priori, more complicated to calculate. Averages of products of four operators at two different times have to be performed. This task becomes much simpler for the case of zero time delay. $g^{(2)}(t; = 0)$ is a one-time operator, which simplifies the calculation. In spite of losing information, $g^{(2)}(t; = 0)$ is a very interesting magnitude because it can be used as indicator of the possible coherence of the state of the system [1, 2, 3, 4]. In addition, if we concentrate in the properties of cavity modes (i.e., neglecting the emission of leaky modes), the second order coherence function acquires a very simple form in the stationary limit:

$$\begin{aligned} g^{(2)}(t; = 0) &= \frac{h a^y a^y a a i}{p h a^y a i^2} \\ &= \frac{n(n-1) [X_{n;X_n} + G_{n;G_n}]}{[n [X_{n;X_n} + G_{n;G_n}]]^2}; \end{aligned} \quad (28)$$

$g^{(2)}$ takes different values depending on the statistics of the photon state: $g^{(2)} = 2$ for chaotic states, $g^{(2)} = 1$ for states having a Poisson distribution in n , and $g^{(2)} < 1$ for non classical systems having a sub-Poisson distribution [2, 3, 4].

III. RESULTS

A. Election of the range of parameters of interest

Since our model has several parameters, we need some simple picture in order to get insight on the interesting regime of parameters. Although our system is similar to a spin coupled to an harmonic oscillator, we can understand the effect of dissipation by considering two-coupled (by g) oscillators. One of them has an eigenfrequency ω_X being damped with a rate γ while the other, with an eigenfrequency ω_G , is damped with a rate γ and is pumped incoherently with a rate P . The incoherent pumping implies a dephasing mechanism which, together with the damping, gives an average dephasing

$(\gamma + P)/2$. When the damping of the first oscillator is much higher than the dephasing $(\gamma + P)/2$ of the second oscillator, one could expect that the frequency of this second oscillator ω_X will survive longer than ω_G and it will dominate the spectrum. In the opposite limit, $(\gamma + P)/2$, the frequency ω_X will dominate the spectrum. This behavior is the one shown by our spin-oscillator system as can be checked by means of the Haken's model on adiabatic elimination [2, 3, 15] in the equations of motion of the field operators. From this simple picture we can motivate the existence of three different regimes $(\gamma + P)/2 < \gamma$, $(\gamma + P)/2 = \gamma$ and some intermediate regime. For this purpose, we fix $g = 1$ as the energy scale, take a fixed small value $\gamma = 0.1$ reflecting the fact that leaky modes emission is the less efficient mechanism in practical situations, and define the three regimes by changing P and ω_X .

Apart from those parameters, our model requires to set the frequency of the two oscillators. In practical cases, the coupling between the oscillators is in the order of meV while the excitation energy ω_X is in the order of eV. Therefore, since our energy scale is $g = 1$ (meV), all the calculations we present here have been performed by taking $\omega_X = 1000$. Finally the detuning Δ is a very important parameter. Since typical detunings are in the order of a few meV, we present here results for two different cases: perfect resonance, $\Delta = 0$ and quasi-resonance $\Delta = 5$.

B. Dynamics of the density matrix: occupations and coherences

In this subsection we show the time evolution of the occupations and coherences (diagonal and off-diagonal respectively) $\rho_{in;jm}$ described in Eqs. (9), (10) and (11). From these equations, it is clear that if losses and pumping are not included, the system shows the usual Rabi oscillations in each subspace with a given number of photons. The amplitude of these oscillations increases with the coupling, g , and decreases with the detuning Δ .

When all the losses and the pumping are included, the situation changes drastically. The initial occupation of $|jG0\rangle$ evolves with time up to a state of equilibrium in which occupation is redistributed among a large number of levels with a finite number of photons. In this final steady situation, the sum of all the losses equilibrates the pumping.

Figs. 2 and 3 show the time evolution of occupations $\rho_{in;jn}$ for both the exciton ($i = X$) and the ground ($i = G$) states. The results in Figs. 2 and 3 are typical of the two extreme regimes described above. When pumping rate P dominates (Fig. 2), states with a large number of photons n become occupied and two bundles of branches can be distinguished: upper branches corresponding to $|jXn\rangle$ states and lower branches corresponding to $|jGn\rangle$ states. In any case, the differences between the occupations of states in the two bundles, is not very

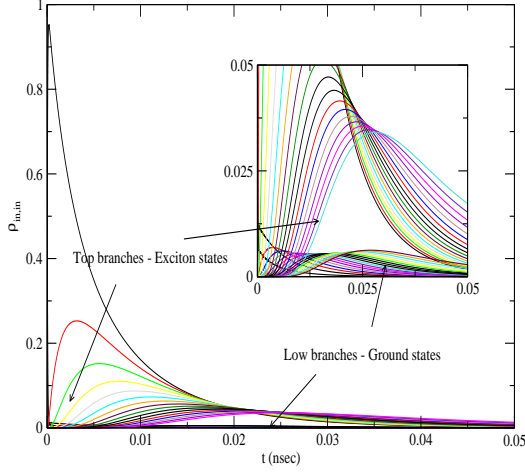


FIG. 2: Density matrix diagonal elements $\rho_{in,in}$ for both the exciton ($i = X$) and the ground ($i = G$) states, from $n = 0$ up to $n = 35$ cavity photons. $g = 1$, $\gamma = 5$, $\kappa = 0.1$, $\Delta = 0.1$ and $P = 15$. The inset shows a zoom of the graphic to clarify the formation of two bundle of branches associated with the exciton and the ground states of the QD respectively.

large. When rates for losses increase and become comparable to the pumping rate, just a few photons can be stored in the cavity. In equilibrium, the highest occupation is that of the $|G0\rangle$ state and only states with $n < 3$ have appreciable, although small, occupations. It is quite evident that an interesting regime is missing in these results: the one in which losses dominate onto the pumping, for instance the case $\gamma = 5$ and $P = 1$. We will discuss below other characteristics of this case but do not include a figure here because the corresponding time dependence is featureless showing a fast decay to zero of the occupations for all the states with $n > 0$.

The time evolution of coherences $\rho_{0,G1}$ is shown in Fig. 4 for the two limiting cases $P \rightarrow 0$ and $P \rightarrow \infty$ for $\gamma = 5$. Due to this finite detuning, Rabi-like oscillations appear in the coherences. When $\kappa \rightarrow 0$, the coherences increase with time up to finite, but small, value. When pumping dominates, the mean number of photons inside the cavity is much higher than 1 as discussed below. Therefore, a coherence like the one in Fig. 4 between states with $n = 0$ and $n = 1$ decreases with time. In this case, $P \rightarrow \infty$, we have computed coherences $\rho_{n,Gn+1}$, for values of n around the mean number of photons inside the cavity (see below), obtaining that they also go to a small constant (apart from the Rabi oscillations) for large times.

All the results included in Figs. 2, 3 and 4 correspond to a finite detuning $\Delta = 5$. In the case of perfect resonance $\Delta = 0$, the main effect is the lack of oscillations as shown, as an example, in Fig. 5 for the coherences

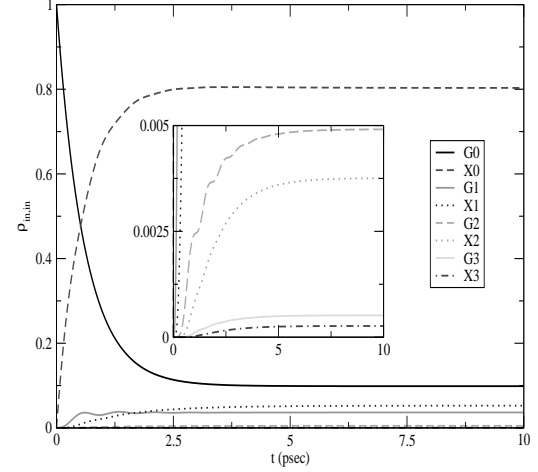


FIG. 3: Density matrix diagonal elements $\rho_{in,in}$ for both the exciton ($i = X$) and the ground ($i = G$) states, from $n = 0$ up to $n = 3$ cavity photons. $g = 1$, $\gamma = 5$, $\kappa = 0.1$, $\Delta = 0.5$ and $P = 1$. The inset shows a zoom of the vertical axis of the graphic.

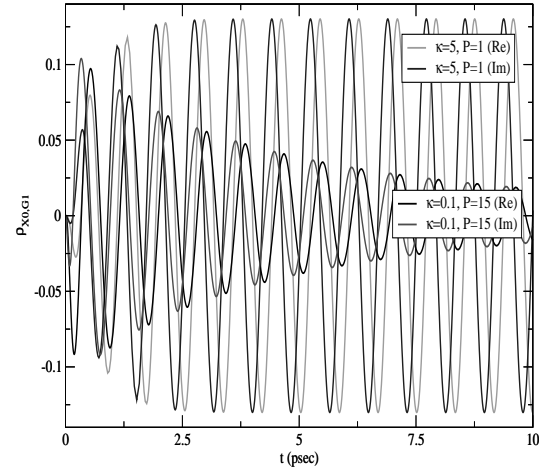


FIG. 4: Density matrix off-diagonal element $\rho_{X0,G1}$ with detuning $\Delta = 5$ for $g = 1$, $\gamma = 0.1$; and two different values of κ and P .

$\rho_{X0,G1}$.

The fact, shown above, that P competes with γ , is not completely general. This fact can be seen in equations (9), (10) and (11) for the time evolution of the density matrix elements. For the off-diagonal terms, P has the same sign than the losses γ and κ , while for the diagonal

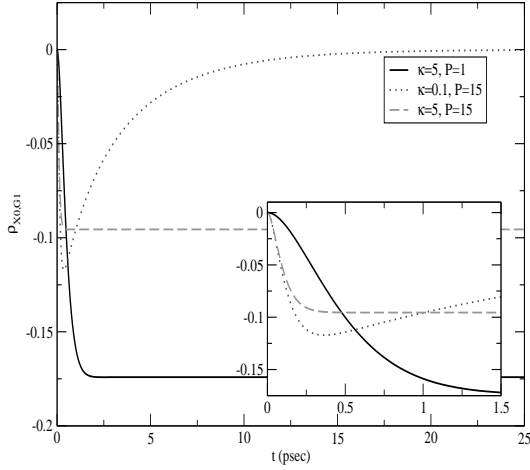


FIG. 5: Imaginary part of the density matrix diagonal element $\rho_{x_0;G1}$ at perfect resonance ($\Delta = 0$) for $g = 1$, $\Delta = 0.1$; and different values of κ and P . All the real parts of the same matrix elements are zero. The inset shows a zoom of the graphic for small values of t .

terms, these signs are different. The pumping produces decoherence in the off-diagonal terms as the emission of photons does because in our model the pumping is incoherent. At the same time, P favors higher occupations (increase of the diagonal elements). Therefore it is clear that, for a high pumping, decays of the off-diagonal terms (loss of coherence) prevail on the occupation until the coherence is completely quenched and later inverted, preventing the evolution towards the occupation of states with a high number of photons. This is an indication of the important role that off-diagonal elements play in the time evolution. It also explains that, if the emission rate is above a critical value, it dominates on any pumping effect.

C. Number of cavity photons

A very important result to be drawn from the time evolution discussed above is the fact that the system is able to store a significant number of cavity photons. Let us analyze the mean number of cavity photons as a first step to study the quantum properties of these photons by looking to its distribution. The mean number of photons in the cavity is

$$\overline{N}_{ph} = \sum_n n (\langle x_n; x_n \rangle + \langle G_n; G_n \rangle) \quad (29)$$

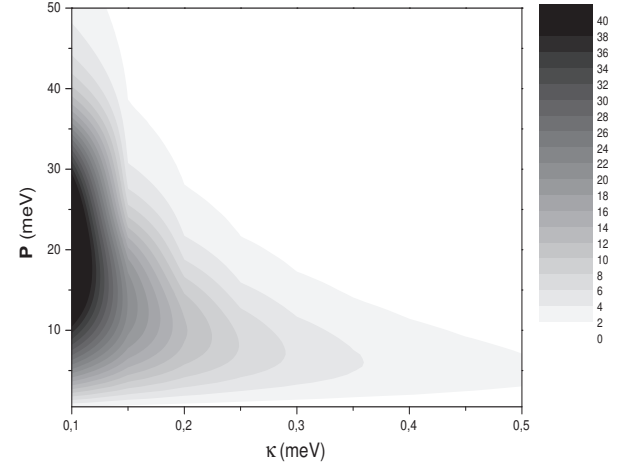


FIG. 6: \overline{N}_{ph} , in grey scale, as a function of κ and P for perfect resonance $\Delta = 0$ with $g = 1$ and $\Delta = 0.1$.

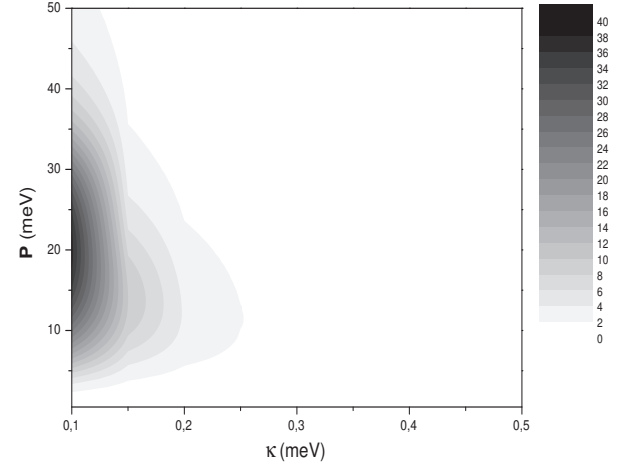


FIG. 7: \overline{N}_{ph} , in grey scale, as a function of κ and P for a detuning $\Delta = 5$ with $g = 1$ and $\Delta = 0.1$.

\overline{N}_{ph} increases with time, in a scale of hundreds of picoseconds, up to the stationary value that is the magnitude we are interested in. Figs. 6 and 7 show a contour plot of the mean number of cavity photons for $\Delta = 0$ and $\Delta = 5$ respectively. As in previous figures, we fix all the parameters except P and κ , which vary along the two axis. In these figures a region with a high \overline{N}_{ph} can be observed. It corresponds to low emission and high

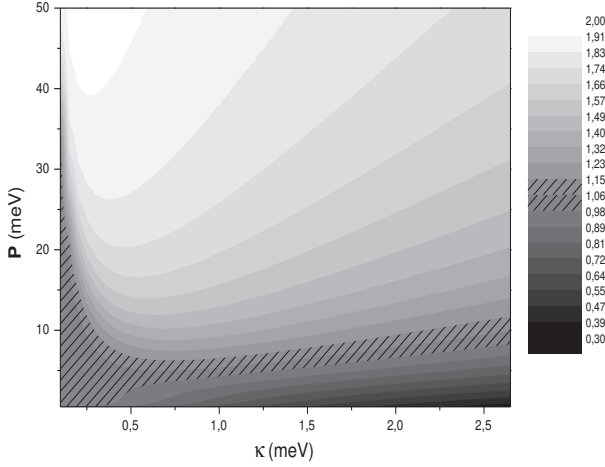


FIG. 8: Second order coherence function $g^{(2)}(\tau = 0)$, in grey scale, as function of κ and P for perfect resonance $\Delta = 0$. $g = 1$ and $\gamma = 0.1$. The dashed area shows the region supporting a Poisson distribution of cavity photons in which $g^{(2)}(\tau = 0)$ close to 1.

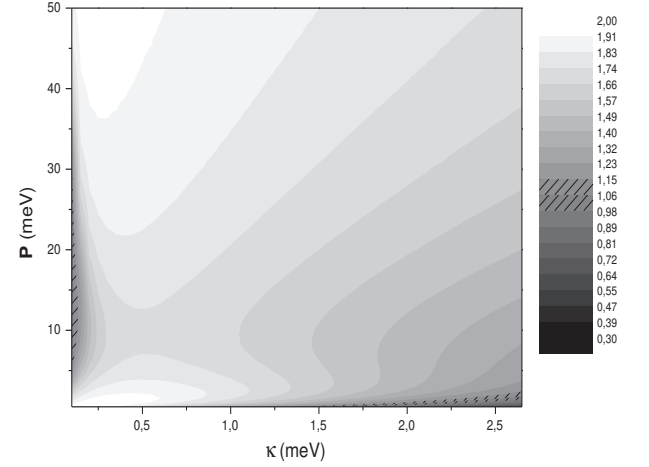


FIG. 9: Second order coherence function $g^{(2)}(\tau = 0)$, in grey scale, as function of κ and P for a detuning $\Delta = 5$. $g = 1$ and $\gamma = 0.1$. The dashed area shows the region supporting a Poisson distribution of cavity photons in which $g^{(2)}(\tau = 0)$ close to 1.

pumping. The region is larger and the number of cavity photons higher for the resonant case, $\Delta = 0$, than for the case with detuning $\Delta = 5$. A detuning makes more difficult the coupling between the states $|j, N\rangle$ and $|j, N+1\rangle$. As a consequence the mechanism of storing cavity photons become less efficient.

A conclusion similar to the one drawn in the previous section is in order: when pumping increases, the mean number of cavity modes also increases up to a certain maximum value. Further increase of P implies that the dephasing mechanism related with this incoherent pumping provokes a decrease of N_{ph} .

D. Second order coherence function

The possibility of storing a large number of cavity photons for a wide range of parameters opens an interesting alternative beyond the simple value of N_{ph} : how is the distribution of cavity photons? If any interesting distribution is involved, its character could be transferred to the light emitted by the system.

In order to quantify if such distributions are closer to gaussian distributions (thermal or chaotic states), Poisson distributions or even non-classical sub-poissonian distributions, one can compute, using Eq. (29), the second order coherence function $g^{(2)}(\tau = 0)$ discussed above.

Figs. 8 and 9 show $g^{(2)}(0)$, for $\Delta = 0$ and $\Delta = 5$ respectively. In these two figures we have dashed the region in which $g^{(2)}(0)$ is close to 1 to show the region

supporting a poissonian distribution. This is the border between classically accessible region and the one having $g^{(2)}(0) < 1$ with non-classical states with sub-poissonian distribution. In the case of perfect resonance (Fig. 8), for low κ , the poissonian distribution region is rather wide in terms of the pumping P . When κ increases, this region becomes much narrower in P . In the case of detuning $\Delta = 5$, the poissonian region becomes much smaller and even disappearing for intermediate values of κ .

The interesting region of $g^{(2)}(0) < 1$ appears for very low pumping in these two figures. Even though this occurs in a small region of parameters, it is very interesting because it means that the system can form squeezed photon states with sub-poissonian distribution. In this region the emitted light shows the antibunching that is characteristic of non-classical light emitters.

The rest of the diagram is supporting states with $g^{(2)}(0)$ increasing from 1 to 2, i.e. states where second order coherence is reduced and approaching a gaussian distribution ($g^{(2)}(0) = 2$). A finite detuning enlarges this gaussian region as observed when comparing the two figures.

Combining and summarizing the results of Figs. 6, 7, 8 and 9, it must be stressed that, for high quality cavities, i.e. low κ and γ , and intermediate value of the incoherent pumping P is able to produce a rather large number of cavity photons with Poisson distribution. When detuning increases this effect remains, although with a reduction of the region of parameters supporting it.

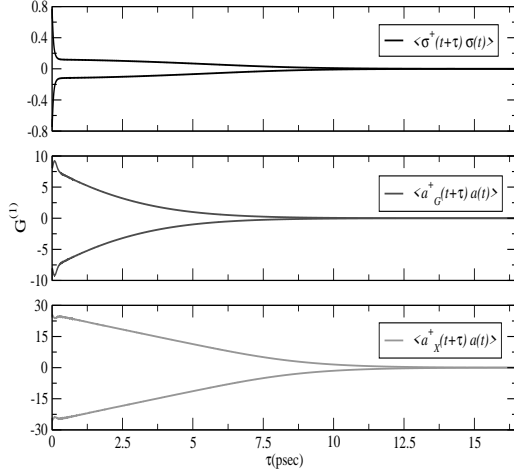


FIG. 10: Envelope of the first order correlation functions $G_X^{(1)}(\tau)$ (upper panel) and $G_C^{(1)}(\tau)$ (two lower panels) at the stationary limit ($t \rightarrow \infty$). $g = 1$, $\gamma = 5$, $\kappa = 0.1$, $\beta = 0.1$ and $P = 15$.

IV. SPECTRUM OF THE EMITTED LIGHT

In this section we will present our results for the spectrum of the emitted light in the stationary limit ($t \rightarrow \infty$). This is the property that can be most easily measured in experiments. We will do it only in the case of finite detuning $\Delta = 5$ in order to observe the emission at two different frequencies. Following the steps discussed in the section devoted to our model, we have computed $G_X^{(1)}(\tau)$ and $G_C^{(1)}(\tau)$ in the stationary limit ($t \rightarrow \infty$) for the three regimes already discussed P_{cav} , P_{leak} and P_{comp} comparable to γ . The envelopes (with fast oscillations inside) of these functions are shown in Figs. 10, 11 and 12 in which we show different contributions to the total emission. In these three figures, the upper part shows the spontaneous emission of leaky modes ($G_X^{(1)}(\tau)$), while the two lower parts show two different contributions to the stimulated emission through cavity modes ($G_C^{(1)}(\tau)$). Fig. 10 correspond to a case with a large N_{ph} inside the cavity. Therefore, when summing up in order to get $G_X^{(1)}(\tau)$ and $G_C^{(1)}(\tau)$, one obtains a time scale significantly larger than in the case of Figs. 11 and 12, which correspond to a small N_{ph} inside the cavity.

The Fourier transform of Figs. 10, 11 and 12 gives the spectrum of the light emission in the three cases discussed above. In order to numerically perform such Fourier-transforms, we have used digital data filters (Parzen and Hanning) to reduce numerical noise. The spectra corresponding to $N_{\text{ph}} = 1000$ are shown in Figs. 13, 14 and 15. In these three figures we have made use of the fact,

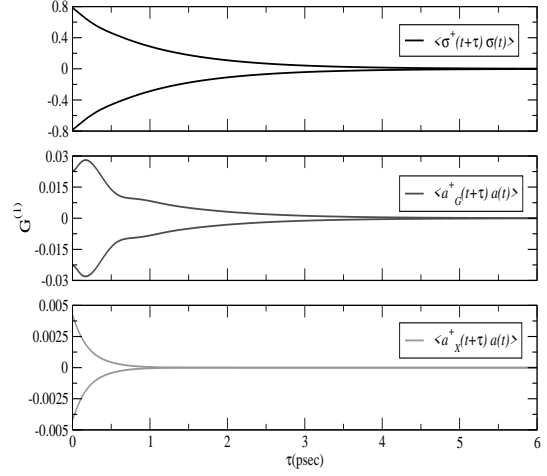


FIG. 11: Envelope of the first order correlation functions $G_X^{(1)}(\tau)$ (upper panel) and $G_C^{(1)}(\tau)$ (two lower panels) at the stationary limit ($t \rightarrow \infty$). $g = 1$, $\gamma = 5$, $\kappa = 0.1$, $\beta = 5$ and $P = 1$.

discussed in the introduction, that the two types of emission can be separated: the emission coming from the cavity modes takes place along the axis of the pillars, while the emission of leaky modes takes place in any spatial direction (mainly in the directions perpendicular to the axis of the pillar).

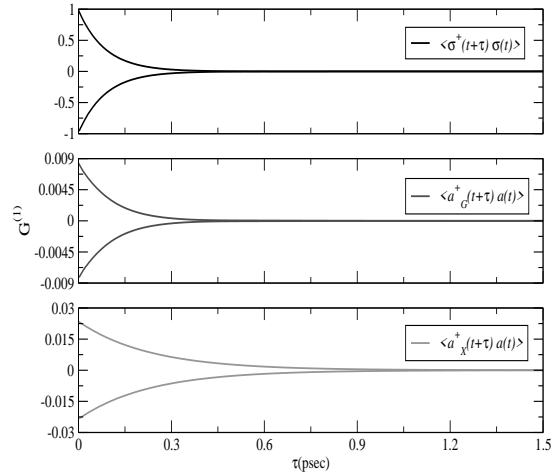


FIG. 12: Envelope of the first order correlation functions $G_X^{(1)}(\tau)$ (upper panel) and $G_C^{(1)}(\tau)$ (two lower panels) at the stationary limit ($t \rightarrow \infty$). $g = 1$, $\gamma = 5$, $\kappa = 0.1$, $\beta = 5$ and $P = 15$.

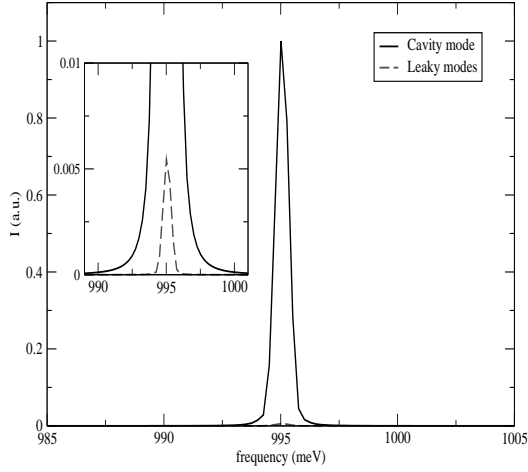


FIG. 13: Spectrum of emission for $g = 1$, $\gamma_x = 1000$, $\gamma = 5$, $\gamma_0 = 0.1$, and $P = 15$.

The case of Fig. 13 corresponds to a high pumping dominating on the effect of γ . As discussed above, one expects a strong damping of the oscillator with frequency γ_x . Therefore, only one peak at γ_x is observed. Moreover, the peak shown in this spectrum is significantly narrower than the features observed in any other case we have analyzed as, for instance, the ones in the following figures.

Fig. 14 shows the result with a high value of the rate emission $\gamma = 5$ and a smaller, although non negligible, pumping $P = 1$. This case corresponds to $N_{ph} = 0.027$ and $g^{(2)}(0) = 0.396$, i.e. to a sub-poissonian distribution of a small number of cavity photons. Now, the strong damping of the mode with frequency γ_x reduces its intensity which becomes smaller than a second peak at γ_0 .

In the intermediate case shown in Fig. 15, the dephasing of the two modes is similar and this produces a very wide peak at the spectrum as observed in the figure.

Let us finally analyze more carefully the case of high quality cavity (already studied in Fig. 13). For this purpose, we maintain fixed a low value $\gamma_0 = 0.1$ and let the pumping vary in a wide range of values. Figs. 16 and 17 show the spectra of the stimulated (cavity) and spontaneous (leaky) emissions respectively. First of all one must observe that scale in Fig. 16 is more than 200 times larger than that of Fig. 17 as it could be expected from the results and discussion of Fig. 13. The main result to be drawn from Figs. 16 and 17 is that the most intense emission corresponds to the range $10 \leq P \leq 30$ simply because this is the range of higher number of photons inside the cavity as shown in Fig. 7.

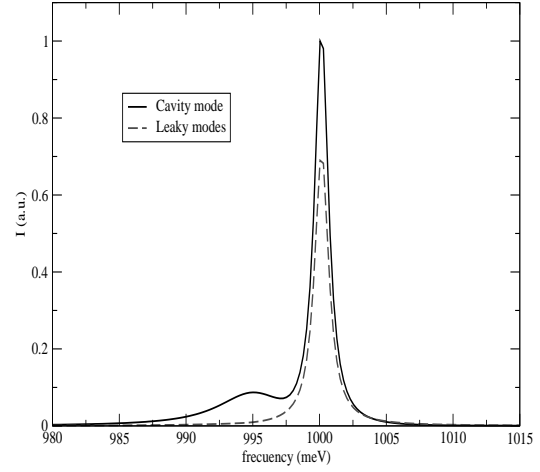


FIG. 14: Spectrum of emission for $g = 1$, $\gamma_x = 1000$, $\gamma = 5$, $\gamma_0 = 0.1$, $\gamma = 5$ and $P = 1$.

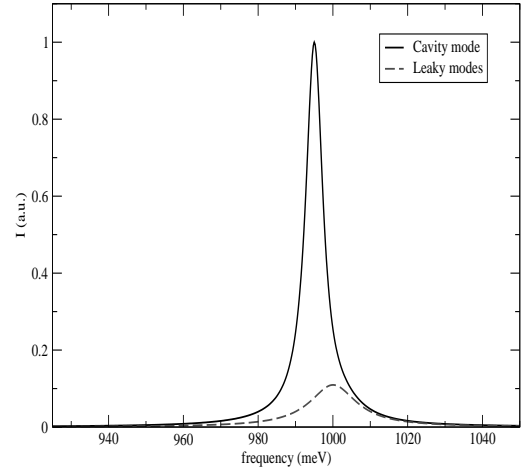


FIG. 15: Spectrum of emission for $g = 1$, $\gamma_x = 1000$, $\gamma = 5$, $\gamma_0 = 0.1$, $\gamma = 5$ and $P = 15$.

V. SUMMARY

We have described the dynamics of a QD embedded in a semiconductor microcavity by means of a two-level system strongly coupled to a single cavity mode. The system is continuously excited by incoherent pumping of excitons. Two different sources of photon emission are considered: spontaneous emission through a leaky mode and stimulated emission of a cavity mode escaping from

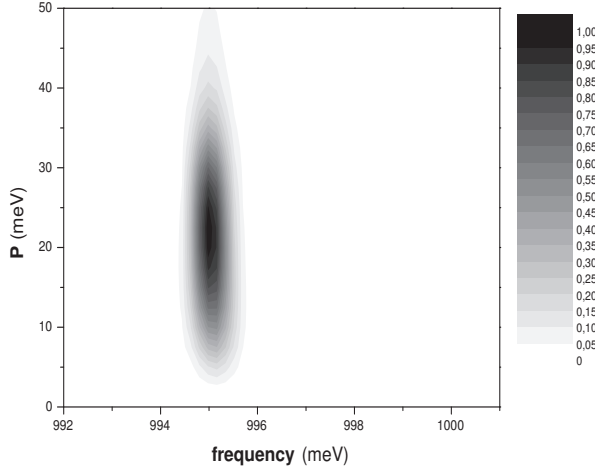


FIG. 16: Spectrum, in grey scale, of stimulated emission (cavity modes escaping from the cavity) as a function of frequency and P . $g = 1$, $\omega_x = 1000$, $\gamma = 5$, $\alpha = 0.1$ and $\beta = 0.1$.

the cavity. The time evolution of first and second order coherence functions is calculated. When pumping dominates over emission rates, a large number of cavity photons can be stored in the cavity. Further increase of the pumping introduces dephasing and a decrease of the number of cavity photons. These different regimes are also characterized by poissonian or gaussian photon distributions inside the cavity. Sub-poissonian distributions can be obtained for a range of parameters, in which the pumping rate is very small, and the quantum nature of the QD-cavity system manifests itself in the emitted light. Finally, we have studied the emission spectrum of our system. In the case of high pumping dominating on the rate emission, one gets a strong damping of the oscillator corresponding to the exciton level with frequency ω_x , and only one very narrow peak at ω_x is ob-

served. When the rate emission is higher than a non negligible pumping rate P , the strong damping of the mode with frequency ω_x allows to observe the two modes with a higher intensity for the mode at ω_x . In an intermediate case, the dephasing of the two modes is similar producing a very wide peak at the spectrum.

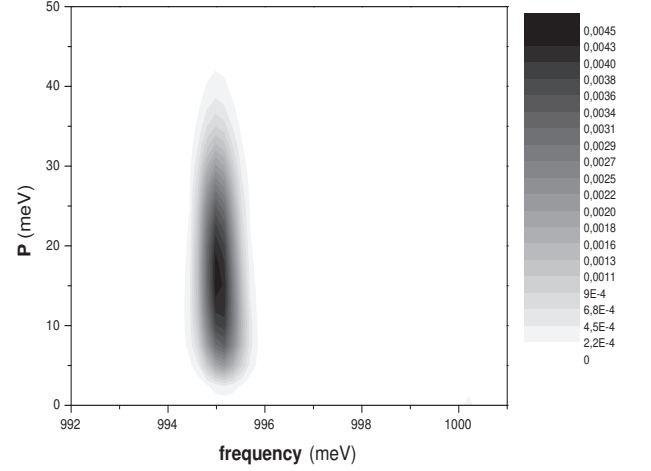


FIG. 17: Spectrum, in grey scale, of spontaneous emission (emission of leaky modes) as a function of frequency and P . $g = 1$, $\omega_x = 1000$, $\gamma = 5$, $\alpha = 0.1$ and $\beta = 0.1$.

VI. ACKNOWLEDGEMENTS

We are indebted to Dr. P. Hawrylak for helpful discussions within the framework of the CERION2 project. Work supported in part by MCYT of Spain under contract No. MAT2002-00139 and CAM under Contract No. 07N/0042/2002. The numerical work has been carried out in part at the CCC of UAM within the project QUANTUMDOT.

[1] C. Cohen-Tannoudji, J. Dupont-Roc and G. Grynberg, Atom-photon interactions, (Wiley-Interscience, New York, 1992).
 [2] D.F. Walls and G.J.M. Milburn, Quantum optics, (Springer-Verlag, Berlin, 1994).
 [3] M.O. Scully and M.S. Zubairy, Quantum optics, (Cambridge University Press, Cambridge, 1997).
 [4] Y. Yamamoto and A. Imamoğlu, Mesoscopic quantum optics, (Wiley, New York, 1999).
 [5] J.M. Gerard, et al., Phys. Rev. Lett., 81, 1110 (1998).
 [6] O. Benson, et al., Phys. Rev. Lett., 84, 2513 (2000).
 [7] P. Michler, et al., Science, 290, 2282 (2000).

[8] G.S. Solomon, et al., Phys. Rev. Lett., 86, 3903 (2001).
 [9] E. Moreau, et al., App. Phys. Lett., 79, 2865 (2001).
 [10] C. Santori, et al., Nature (London), 419, 594 (2002).
 [11] M. Pelton, et al., Phys. Rev. Lett., 89, 233602 (2002).
 [12] T.M. Stace, et al., Phys. Rev. B, 67 085317 (2003).
 [13] A.V. Kozlovskii and A.N. Oraevskii, JETP, 88, 666 (1999).
 [14] O. Benson and Y. Yamamoto, Phys. Rev. A, 59, 4756 (1999).
 [15] G.W. Gardiner Handbook of stochastic methods, (Springer-Verlag, Berlin, 1983).